Citation
Jin, H. and Hao, H. and Hao, Y. and Chen, W. 2020. Predicting the response of locally resonant concrete structure under blast load. Construction and Building Materials. 252: ARTN 118920.
http://doi.org/10.1016/j.conbuildmat.2020.118920

Predicting the response of locally resonant concrete structure under blast load

Hexin Jin[a,b], Hong Hao[b*], Yifei Hao[a], Wensu Chen[b]

[a] School of Civil Engineering, Tianjin University, Tianjin 300350, China

[b] Centre for Infrastructural Monitoring and Protection, School of Civil and Mechanical Engineering, Curtin University, Australia

[*]**Corresponding author**

Abstract

Ternary locally resonant metamaterial (LRM) is a manmade material consisting of rigorously designed heavy inclusions with coated soft layer. Such design enables the LRM to possess good wave-filtering characteristics that differ from the matrix materials. Researches of application of this new material for seismic isolation and sound insulation in civil engineering have been reported. In recent decades, there has been an increasing demand to protect civil engineering structures against the effects of blast loading. When blast wave acts on a concrete structure, complex stress waves are generated and propagate in the structure. The wave-filtering characteristics of LRM have brought inspiration to investigate its potential application to reduce the stress wave propagation and hence the damage to cementitious material and enhance the performance of structures under blast wave. By embedding heavy inclusions with soft coating layer into mortar matrix, the product can be named as ternary locally resonant concrete (ternary LRC). Previous studies of the performances of ternary LRC structures are mainly limited to finite element (FE) modeling of elastic wave propagation. The study of the performance of ternary LRC structure subjected to blast loading and the influence of blast loading-induced damage to LRC structure on stress wave propagation is very limited. This paper carries out analytical derivation and numerical modelling to study the mechanism and performance of ternary LRC structure under blast loading. The strain rate effect and material damage of the mortar matrix are considered in numerical simulation. The influence of different material inclusions (natural aggregates and lead), different elastic modulus and thickness of the soft coating on the response of ternary LRC structure are studied. The results show that the ternary LRC can effectively reduce the damage of ternary LRC structure subjected to blast loading.

Key words: Ternary locally resonant concrete; Blast loading; Analytical prediction; Numerical simulation

1. Introduction

Metamaterial is the general term of composite materials consisting of artificially designed components and exhibiting physical properties that are not possessed by the matrix materials. The idea of metamaterial was first introduced in the field of electromagnetism, such as electromagnetic absorbers, which can stop the propagation of electromagnetic waves in certain frequency regimes [1-3], namely band gaps.

Due to the mathematical analogy among acoustic wave, elastic wave and electromagnetic wave, some researchers have attempted to find acoustic or elastic metamaterials possessing similar properties [4-7]. These metamaterials are divided into two categories: Bragg-type metamaterials and locally resonant metamaterials (LRM). These two metamaterials provide band gaps based on different mechanisms. For Bragg-type metamaterials, the interaction between artificial structures or the periodicity of structures plays a dominant role. To generate band gaps in the low frequency range, the internal artificial structures need to have spatial periodicity and the size of artificial structures needs to be similar to the wavelength of the incoming wave. However, since the wavelength of low-frequency waves in solids is generally long (from a few decimeters to hundreds of meters), the use of Bragg-type metamaterial alone to block low-frequency loads in civil engineering has certain inherent restrictions [8]. In year 2000, the very first LRM was invented by Liu et al. [9], who embedded lead spheres coated with silicone rubber into an epoxy matrix, which overcame the limitation of Bragg-type metamaterials on the size of structures. When an elastic wave passes through the material, the internal lead sphere resonates at its natural frequency, storing energy applied to the material and producing band gaps caused by resonance. With the same geometry, LRM exhibits band gaps in a frequency range two orders of magnitude lower than Bragg-type metamaterial [10].

Following Liu's work [9], lots of other forms of LRM have been proposed. These existing LRM can be further divided into two categories: the binary LRM and the ternary LRM. The binary LRM is a kind of metamaterial made of hard matrix with soft inclusions. For instance, Hsu and Wu [11] successfully made a kind of binary LRM plate by putting periodic soft rubber fillers into epoxy matrix, and studied the effect of binary LRM on the Lamb wave propagating in the plate. The ternary LRM consists of heavy inclusions coated with soft coating and embedded into the hard matrix. Li and Chen [12] developed a kind of ternary LRM by incorporating the lead spheres coated with rubber into short fiber reinforced cementitious matrix.

At the present stage, this novel concept has attracted broad attentions from civil engineering researchers for structural protection against dynamic loads, mainly earthquakes. By using this material as the foundation of structure, the energy of seismic waves can be reduced or obstructed [13-15]. Yan et al. [14] built a structure with a scaled LRM periodic foundation to verify the effectiveness of the foundation on mitigating the earthquake ground excitations to the building structures. Test results indicated that LRM periodic foundation was a feasible approach to reduce structural vibrations under seismic actions. Asiri and Alzahrani [15] used LRM to build some one-dimensional layered periodic structures to reduce the response of platforms in offshore structures.

In recent decades, the exposure of building structures to blast threats extends beyond war zones. Civilian structures also face the increased safety risk due to the rising number of accidental explosions and/or terrorist bombing attacks on important governmental and civilian facilities. Blast loading is characterized with extremely short duration, high frequency and high intensity, which results in different structural responses as compared to those from static and less intense dynamic loads such as earthquake, wave and wind loads [16]. Consequences of these extreme loading events could be catastrophic, involving extensive casualties, significant damage to structures, extraordinary economic loss and immeasurable social disruption. For structural and personnel protection against explosive loads, the explosion hazards in protective design are normally referred to the blast overpressure acting on the structures or people. When a blast load acts on a concrete structure, it generates large stress waves propagating in the structure. When the blast-induced compressive stress wave reaches the back face of the structure, it reflects and the reflected stress wave induces tensile stress on the back face of the structure, which may lead to severe spall damage of concrete with flying fragments because of the brittleness and very low tensile strength of concrete [17].

The current protective technology adopts obstacles, such as fence wall [18], solid wall [19], and ring mesh with water fall [20], in front of structures to mitigate blast loadings, or strengthen the concrete structure with FRP materials [21, 22], or providing sacrificial layers for primary structure protections [23]. Pioneering studies have also been conducted by some researchers to investigate the possibility of using ternary LRM to effectively attenuate the stress waves caused by blast loading, and hence mitigate the structural damage. Mitchell et al. [24-26] conducted numerical studies to investigate the effectiveness of embedding lead spheres coated with soft materials into mortar to make ternary locally resonant concrete (ternary LRC) for mitigation of the blast loading effect, and found that the lead spheres can store part of the energy applied by blast loading, reduce the stress carried by the mortar phase, and hence greatly improve the ability of the mortar to resist blast loading. Tan et al. [27] presented the ternary LRC for mitigating the impact and blast loading effects. In the latter study, two kinds of heavy inclusion designs, namely single-layer heavy inclusion and dual-layer heavy inclusion, were proposed. Results evidently demonstrate that dual-layer heavy inclusion can more effectively attenuate blast-wave than the single-layer heavy inclusion. All the above studies demonstrate the effectiveness of LRC in mitigating stress wave propagation and its application potentials for structural protections. However, the studies are very limited, especially on the detailed examinations of the performances and mechanisms of ternary LRC under blast loading. For possible practical applications, further studies are deemed necessary. In addition, it should be noted that most of the previous researches on the mechanical properties of ternary LRC are based on simple harmonic input [28, 29], which are effectively used in examining the performance of ternary LRC structure subjected to idealized wave forms and earthquake loading. The response of ternary LRC structure under blast loading is limited to numerical simulations [24-26] or experimental investigations [30]. There has no analytical derivation of the responses of ternary LRC structures subjected to aperiodic wide band load such as blast loading yet. Analytical solution of responses of ternary LRC structures subjected to blast loads allows straightforward examinations of the performances and mechanisms of ternary LRC designs, and is also handy for bench marking the solutions for verifying the numerical model. In this study, both numerical simulations and analytical derivations are carried out to investigate the performance of ternary LRC structures subjected to blast loads.

On the other hand, large blast load generates nonlinear plastic waves and damages to structures, the previous studies on the effectiveness of ternary LRC on stress wave propagation usually assume idealized elastic wave propagations. The effectiveness of ternary LRC on structure protection against blast and impact load needs be further investigated by taking into consideration the plastic wave and structural damage because structural damage and plastic deformation not only absorb a significant amount of wave energy, but also changes mechanical properties of the structure and hence the wave propagation characteristics.

The present study conducts analytical derivations to predict the response of ternary LRC structure first. By simplifying the ternary LRC structure model as a mass-in-mass system [31], the dynamic response of ternary LRC structure under blast loading is then analytically derived by using the structural dynamics theory of multi-degree-of-freedom (MDOF) system [32]. To study the propagation of stress wave and the destruction of the material in the ternary LRC structure under blast loading, a finite element model of ternary LRC structure is built in LS-DYNA. The results from analytical predictions and FE modelling of the ideal ternary LRC structures are compared with each other first to verify the accuracy of the numerical model. The verified numerical ternary LRC structure model is then extended to include the strain rate effect and the material damage of mortar matrix under high intensity blast loads. The effects of different core materials (i.e., natural aggregate and lead), different thickness and elastic modulus of soft coating on the response of ternary LRC structure are investigated. The coupled effect of material damage and local resonating mechanism in reducing blast wave propagation in ternary LRC structure is studied.

2. Analytical method

The typical ternary LRC structure considered in the present study comprises of spherical lead core, soft coating and mortar matrix. The spherical heavy inclusions are evenly distributed in the mortar matrix, as illustrated in Fig. 1. In the figure, $P(t)$ denotes the input blast overpressure history acting on the structure, d is the distance between centers of two adjacent heavy inclusions, L is the total length of the ternary LRC structure model under consideration, h is the width of cross section of the ternary LRC structure model, R_{i} is the radius of heavy core and b is the thickness of the soft coating. The load action is along the axial direction of the model. The model is simplified as a one-dimensional wave propagation problem, represented by a MDOF mass-in-mass lattice model, as shown in Fig. 2. In the figure, $F(t)$ denotes the input blast force history ($F(t)=P(t)h^2$). The mortar matrix is represented by outer unit cell with mass M and displacement $u_{x,1}(t)$. The heavy core is considered as internal unit cell with mass m and displacement $u_{x,2}(t)$. The mass of the soft coating is ignored in the derivation as it is small compared to that of matrix and heavy core. The connections between outer and internal unit cells are simplified as springs with stiffness k. The connections between outer unit cells are simplified as springs with stiffness K. Three blast loads with the peak value of 5 MPa, 20 MPa and 40 MPa are assumed in the present study (Fig. 3). The 5 MPa peak value is smaller than the compressive strength of mortar, the responses of all materials hence are assumed remaining in the elastic range. This blast loading is used to investigate the performance and mechanism of ternary LRC in mitigating blast wave propagation. The other two blast loads are used to investigate the coupled effect of material damage and local resonating mechanism in mitigating blast waves in ternary LRC structure in the subsequent numerical simulations. These blast loads resemble a realistic air blast load, with negative phase ignored. The material parameters and the geometric parameters of the ternary LRC structure model are given in Table 1-Table 3. Without losing the generality, six lead inclusions regularly distributed in the mortar matrix are assumed.

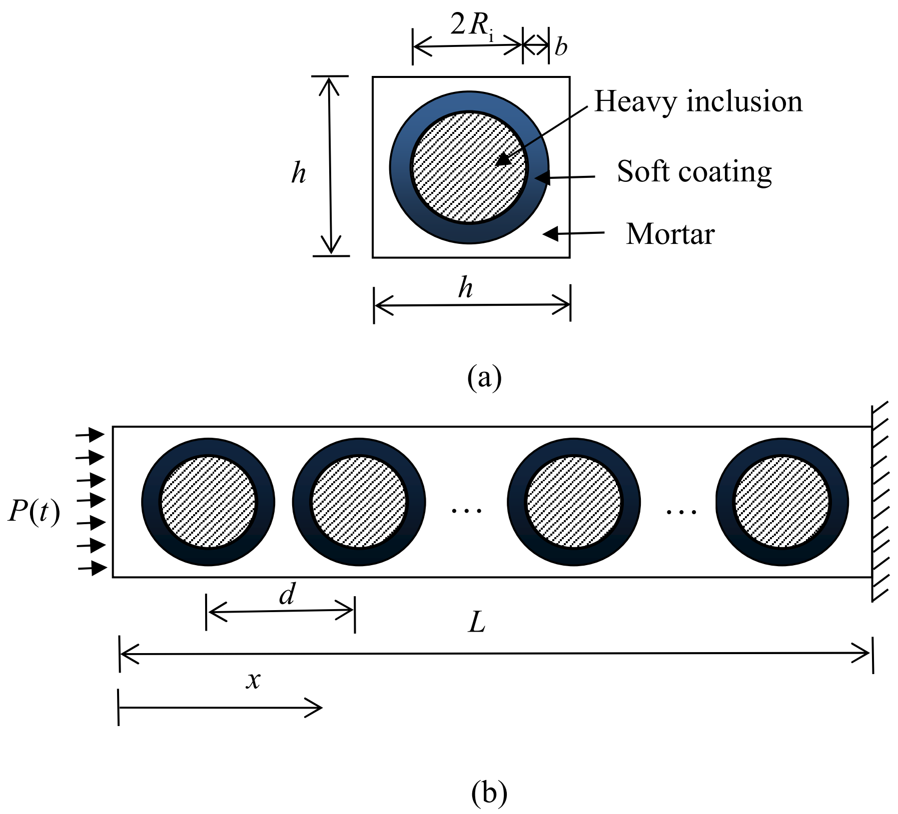

Fig. 1 Illustration of LRC structure model (a) Lateral view, (b) Cross section

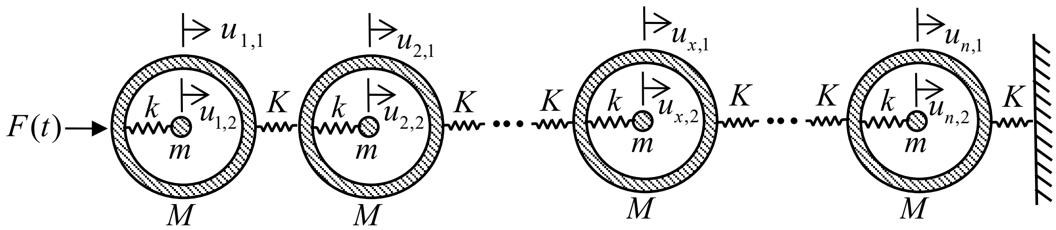

Fig. 2 MDOF mass-in-mass lattice system

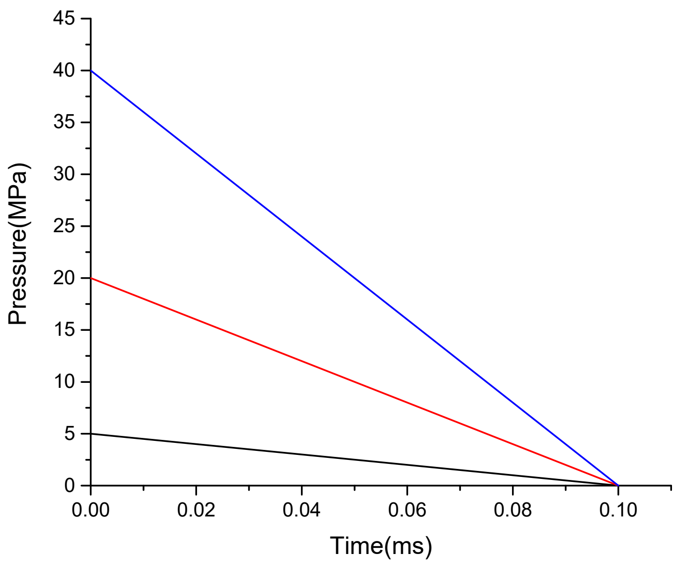

Fig. 3 Blast loading time history

Table 1 Material parameters of mortar [33]

Material	Density (kg/m^3)	Elastic modulus (MPa)	Compressive strength (MPa)	Poisson's ratio
Mortar	2100	3×10^4	34	0.2

Table 2 Material parameters of lead core and polyurethane coating [24]

Material	Density (kg/m^3)	Elastic modulus (MPa)	Poisson's ratio
Lead	11400	1.6×10^4	0.44
Polyurethane	900	1.47×10^2	0.42

Table 3 Geometric parameters of ternary LRC structure

L(m)	d(m)	h(m)	R_i(m)	b(m)

0.24	0.04	0.03	0.009	0.002

By considering the geometric parameters and material parameters of the ternary LRC structure model, the physical parameters of the mass-in-mass MDOF system in Fig. 2 can be calculated by the following formulae.

The mass of the lead core is

$$m = \rho_{\mathrm{i}} \frac{4}{3} \pi R_{\mathrm{i}}^{3} \tag{1}$$

where ρ_{i} is the density of the lead core.

The mass of the outer mortar can be calculated by

$$M = \left[dh^2 - \frac{4}{3} \pi (R_{\mathrm{i}} + b)^3 \right] \rho_{\mathrm{m}} \tag{2}$$

where ρ_{m} is the density of mortar.

The stiffness of the spring connecting the mortar matrix and internal unit cell can be calculated by

$$k = \frac{2 E_{\mathrm{c}} A_{\mathrm{i}}}{b} \tag{3}$$

where E_{c} is the elastic modulus of soft coating, A_{i} is the cross-sectional area of the heavy inclusion [24].

The stiffness of the spring connecting the outer unit cells can be estimated by

$$K = A_{\mathrm{m}} \mu_{\mathrm{m}} / d \tag{4}$$

where A_{m} is the cross-sectional area of the structure and $A_{\mathrm{m}}=h^2$, μ_{m} is the Lame constant of mortar and $\mu_{\mathrm{m}}=\frac{E_{\mathrm{m}}}{2(1+\nu_{\mathrm{m}})}$ [32].

2.1. Motion equation of ternary LRC simplified system under blast loading

To derive the analytical solution for studying the performance and mechanism of ternary LRC in mitigating blast loading, all materials are assumed in the elastic phase. The blast loading with the 5 MPa peak pressure as shown in Fig. 2 acting on the example structure is

$$F(t)=\begin{cases} -4.5\times10^{7}t+4500 & \text{(N)} \quad 0\le t\le 0.0001 \\ 0 & \quad\quad t>0.0001 \end{cases} \tag{5}$$

Neglect damping, the motion equation of the mass-in-mass lattice model is

$$\sum_{i=1}^{n}\sum_{j=1}^{2}(m_{ij}\ddot{u}_{ij}+k_{ij}u_{ij})=F(t) \tag{6}$$

where $m_{i1}=M$, $m_{i2}=m$, $k_{i1}=K$, $k_{i2}=k$.

The above equation can be written in matrix form, i.e.,

$$\boldsymbol{M}\ddot{\boldsymbol{u}}+\boldsymbol{K}\boldsymbol{u}=\boldsymbol{F}(t) \tag{7}$$

where $\boldsymbol{M}$ is the mass matrix of the model, $\boldsymbol{u}$ is the displacement vector, $\boldsymbol{K}$ is the stiffness matrix, and $\boldsymbol{F}$ is the force vector.

The mass matrix can be expressed as

$$\boldsymbol{M}=\begin{pmatrix} M & & & & & & & & & \\ & m & & & & & & & & \\ & & M & & & & & & & \\ & & & m & & & & & & \\ & & & & \ddots & & & & & \\ & & & & & M & & & & \\ & & & & & & m & & & \\ & & & & & & & \ddots & & \\ & & & & & & & & M & \\ & & & & & & & & & m \end{pmatrix} \tag{8}$$

The stiffness matrix can be expressed as

$$
\boldsymbol{K}=\begin{pmatrix}
K+k & -k & -K & 0 & & & & & \\
-k & k & 0 & 0 & & & & & \\
-K & 0 & 2K+k & -k & & & & & \\
0 & 0 & -k & k & & & & & \\
 & & & & \ddots & & & & \\
 & & & & & 2K+k & -k & & \\
 & & & & & -k & k & & \\
 & & & & & & & \ddots & & \\
 & & & & & & & & 2K+k & -k \\
 & & & & & & & & -k & k
\end{pmatrix} \tag{9}
$$

The displacement response vector can be represented by

$$
\boldsymbol{u}=\begin{pmatrix} u_{1,1}(t) & u_{1,2}(t) & \cdots & u_{x,1}(t) & u_{x,2}(t) & \cdots & u_{n,1}(t) & u_{n,2}(t) \end{pmatrix}^{\mathrm{T}} \tag{10}
$$

The non-conservative force vector is

$$
\boldsymbol{F}(t)=\begin{pmatrix} F(t) & 0 & \cdots & 0 & 0 & \cdots & 0 & 0 \end{pmatrix}^{\mathrm{T}} \tag{11}
$$

2.2. Elastic response of ternary LRC system under blast loading

By decoupling Eq. 7, it has

$$
\boldsymbol{M}_{\mathrm{p}}\ddot{\boldsymbol{u}}_{\mathrm{p}}+\boldsymbol{K}_{\mathrm{p}}\boldsymbol{u}_{\mathrm{p}}=\boldsymbol{F}_{\mathrm{p}}(t) \tag{12}
$$

where $\boldsymbol{M}_{\mathrm{p}}$ is the principal mass matrix, $\boldsymbol{K}_{\mathrm{p}}$ is the principal stiffness matrix, $\boldsymbol{u}_{\mathrm{p}}$ is the principal displacement matrix, $\boldsymbol{F}_{\mathrm{p}}(t)$ is the force corresponding to the principal coordinate.

The special solution of the above equations under zero initial conditions is

$$
\boldsymbol{u}_{\mathrm{p}}(t)=\int_0^t \boldsymbol{h}_{\mathrm{p}}(\tau)\boldsymbol{F}_{\mathrm{p}}(t-\tau)d\tau \tag{13}
$$

where $\boldsymbol{h}_{\mathrm{p}}(t)$ is a diagonal matrix with primary coordinate response function $h_{\mathrm{p}j}\,(j=1,2,\cdots,n)$ as element, and

$$h_{pj}(t)=\frac{1}{M_{pj}\omega_j}\sin\omega_j t\,,(j=1,2,\cdots,n) \tag{14}$$

By reversing the principal coordinate, it can be obtained that

$$\boldsymbol{u}(t)=\int_0^t \boldsymbol{h}(\tau)\boldsymbol{F}(t-\tau)\mathrm{d}\tau \tag{15}$$

The sum of kinetic energy and internal energy stored by the lead cores and the polyurethane coatings is

$$te_1(t)=\sum_{i=1}^{n}\left[m\dot{u}_{i2}^{\ 2}+k\left(u_{i,1}-u_{i,2}\right)^2\right]\Big/2 \tag{16}$$

The sum of kinetic energy and internal energy stored by the mortar matrix is

$$te_2(t)=\sum_{i=1}^{n-1}\left[M\dot{u}_{i1}^{\ 2}+K\left(u_{i,1}-u_{i+1,1}\right)^2\right]\Big/2 \tag{17}$$

Fig. 4 shows the displacement $u_{5,1}$ and $u_{5,2}$, i.e., the displacement response of the fifth ternary LRC unit cell, obtained from the analytical solution. It can be seen from the figure that due to the existence of the polyurethane coating, there is a relative movement between the lead core and the mortar matrix. Fig. 5 shows the sum of kinetic energy and internal energy stored by all the coated lead cores and mortar matrix obtained from the analytical solution. As shown, the lead core and the polyurethane coating store a large amount of energy applied to the structure by blast loading. Due to the relative motion between the lead core and the mortar matrix, as shown in Fig. 4, vibration of coated lead cores store a certain amount of energy. Since the total energy in the structure is the same, when the energy stored by the lead core and polyurethane coating increases to a peak value, the energy in the mortar matrix is the minimum. The stress wave intensity in the mortar matrix is thus reduced. These results explain the mechanism on how the ternary LRC mitigates the stress wave propagation in the structure.

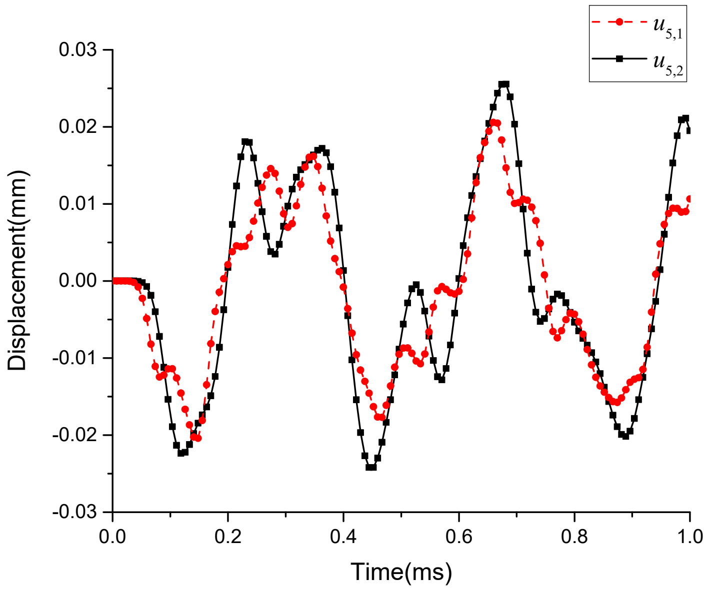

Fig. 4 Displacement time history of $u_{5,1}$ and $u_{5,2}$

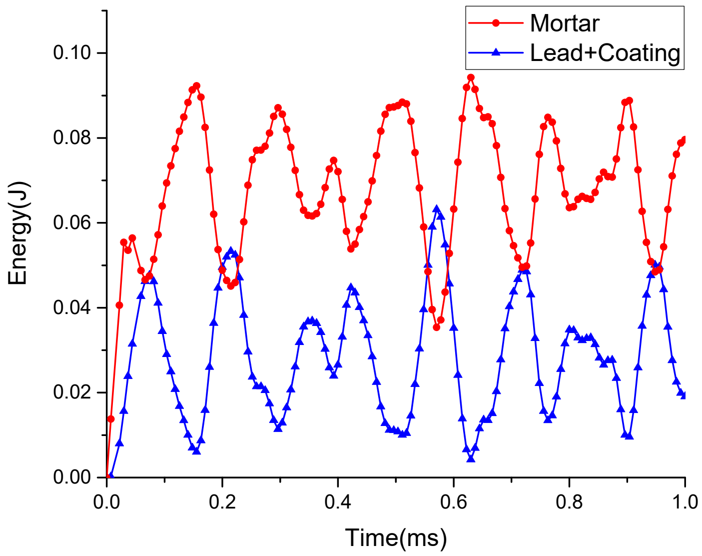

Fig. 5 Energy stored by the coated lead cores and mortar matrix

The above solutions can be easily extended to the cases with different numbers of coated inclusions and solved straightforwardly. They can be used to explain the mechanism on wave energy attenuation in the ternary LRC structures and quantify the energy absorptions of the inclusions.

3. Numerical approach

The above analytical derivation and solution is valid for ideal conditions only, i.e., linear elastic material response and perfect locations of the infilled cells in cement matrix. In practice, under large amplitude blast loadings, cement matrix is likely to experience nonlinear inelastic responses and even suffer severe damages. Moreover, when mixing concrete with the infilled cells, it is difficult to ensure the cells stay at the designated locations. Deriving analytical solution that takes into consideration of the material nonlinearity and damage during stress wave propagation in LRC structure with randomly distributed cells is not straightforward. To overcome this limitation of the analytical solution, a finite element model of ternary LRC structure is built in LS-DYNA in this study for wider and more realistic simulations of the blast load induced stress wave propagations in ternary LRC structures. The analytical solution is used to verify the accuracy of the numerical model.

3.1. Mapping algorithm of finite element model

To generate the finite element model of ternary LRC structure, the following steps are applied:

1. Generate element meshes of the ternary LRC structure specimen;
2. Calculate the central coordinates of each element;
3. According to the geometric design of the model, change the properties of the elements to establish the heavy core and the soft coating.

It should be noted that in the present study the locations of the infilled cells are still assumed at deterministic locations instead of randomly distributed. The influences of randomly distributed infill cells on stopping the stress wave propagations will be studied in the near future.

3.2. Numerical model

Fig. 6a and Fig. 6b show the numerical model and the finite element mesh of the ternary LRC structure composed of six ternary LRC unit cells considered in the above analytical derivation. For comparison, the numerical model of a similar structure without lead inclusion, i.e., pure mortar only is also developed to calculate the stress wave propagations. This model is developed by simply replacing the materials of core and soft coating elements by mortar material. Four sections denoted as Cs1 - Cs4 as illustrated in Fig. 6b are selected to record the wave intensities for examining the effectiveness of wave attenuation in both ternary LRC structure model and pure mortar structure model. A section denoted as Cs5 is selected to record the displacement of lead core and mortar matrix. These five sections (Cs1-Cs5) are located at 5 mm, 40 mm, 80 mm, 235 mm and 180 mm from the front face of the model, respectively. Fig. 7 shows the unit cell of the ternary LRC. In the simulation, the material properties of lead core and polyurethane coating are assumed as linear elastic, while the plastic-damage model for concrete (Mat_72R3) in LS-DYNA is adopted to model the mortar matrix. The material properties are the same as given above in the analytical study.

In this study, an erosion criterion based on the maximum principal strain of 0.15 is used for mortar matrix. The blast loading is applied onto the front face of the model as in the above analytical derivation, as shown in Fig. 6a. The lead core, the polyurethane coating and the mortar are all modeled by solid hexahedron element (Solid 164). Fixed constraints are applied at the end of the model. The contacts between different materials are assumed as perfect bonding, as in the analytical derivation.

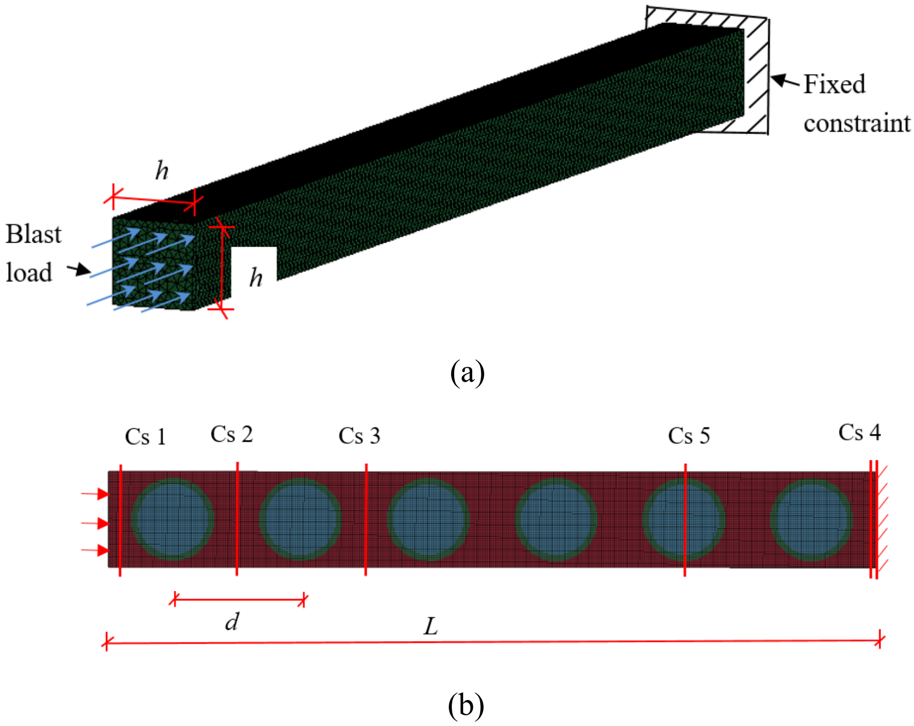

Fig. 6 (a) Considered numerical model, (b) Finite element mesh

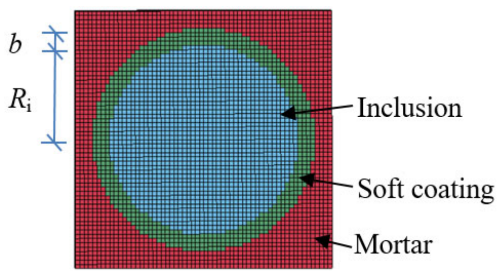

Fig. 7 Cross section of a unit cell of ternary LRC

3.3. Strain rate effect

The strain rate effect on the mortar strength is described by the dynamic increase factor (DIF). In the simulation, the compressive strength DIF for mortar matrix is adopted from Hao et al. [34], which have the lateral inertia confinement effect removed as verified by the experimental data [35]. The tensile strength DIF used for mortar matrix is adopted from Malvar and Crawford [36] and given below.

For compressive strength DIF [34],

$$\text{CDIF}=0.0419(\log\dot{\varepsilon}_{\mathrm{d}})+1.2165\ ,\quad \dot{\varepsilon}_{\mathrm{d}}<30\mathrm{s}^{-1} \tag{18}$$

$$\text{CDIF}=0.8988(\log\dot{\varepsilon}_{\mathrm{d}})^{2}\text{-}2.8255(\log\dot{\varepsilon}_{\mathrm{d}})+3.4907\quad ,\quad 30\mathrm{s}^{-1}\le\dot{\varepsilon}_{\mathrm{d}}\le 1000\mathrm{s}^{-1} \tag{19}$$

For tensile strength DIF [36],

$$\text{TDIF}=(\dot{\varepsilon}_{\mathrm{d}}/\dot{\varepsilon}_{\mathrm{ts}})^{\delta}\ ,\quad \dot{\varepsilon}_{\mathrm{d}}\le 1\mathrm{s}^{-1} \tag{20}$$

$$\text{TDIF}=\beta(\dot{\varepsilon}_{\mathrm{d}}/\dot{\varepsilon}_{\mathrm{ts}})^{1/3}\ ,\quad \dot{\varepsilon}_{\mathrm{d}}>1\mathrm{s}^{-1} \tag{21}$$

where $\delta=1/(1+8f_{\mathrm{cs}}/f_{\mathrm{c0}})$, $\log\beta=6\delta-2$, $f_{\mathrm{c0}}=1\times10^{7}\,\mathrm{Pa}$, $\dot{\varepsilon}_{\mathrm{ts}}=10^{-6}\mathrm{s}^{-1}$ is the static strain rate, f_{cs} is the static compressive strength.

3.4. Mesh size sensitivity analysis

In the finite element analysis, the mesh size affects computational time and accuracy. To optimize the effects of these two factors, a mesh sensitivity test is carried out for the ternary LRC structure model. Three mesh sizes, namely, 0.25 mm, 0.5 mm and 1.0 mm, are considered. The blast loading with the peak value of 20 MPa is used in the mesh size sensitivity analysis. Fig. 8 illustrates the average stress time history on section Cs2 in the ternary LRC structure model corresponding to different mesh sizes. It can be seen that 0.5 mm mesh size yields almost the same prediction as that with the mesh size of 0.25 mm whereas the simulations with the larger element size of 1.0 mm give different predictions. Considering the accuracy and the efficiency for simulation, the finite element model with the mesh size of 0.5 mm is used in this study.

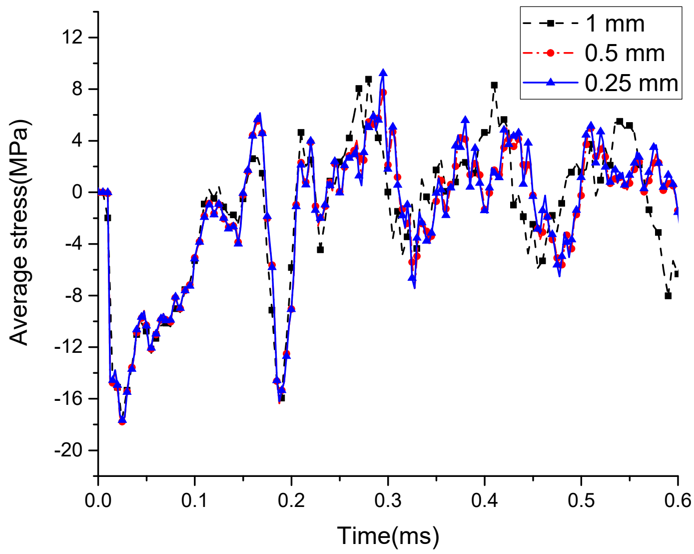

Fig. 8 Influence of mesh size on the average stress time history of section Cs2 in ternary LRC structure model

3.5. Response of ternary LRC structure under blast loading

To verify the numerical model, the ternary LRC structure subjected to 5.0 MPa blast load is simulated as per the analytical study. The numerical simulation results are compared with the results from the analytical solutions. Two elements in section Cs5 as shown in Fig. 9 are selected for comparison, where element 1 and element 2 is mortar element and lead element, respectively.

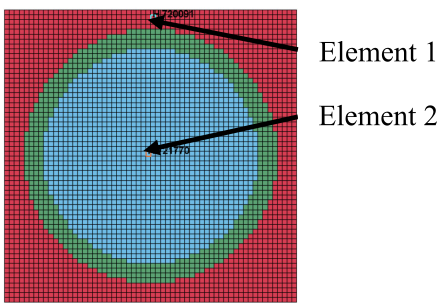

Fig. 9 Location of element 1 and element 2 in section Cs5

Fig. 10 shows the displacements of element 1 and element 2 in ternary LRC structure obtained from analytical solution and numerical simulation. Fig. 11 compares the sum of kinetic energy and internal energy stored by all the lead cores and polyurethane coatings obtained from analytical solution and numerical simulation. It can be seen that the displacement time history and total energy time history obtained from the two methods agree very well, which proves the accuracy of numerical simulation.

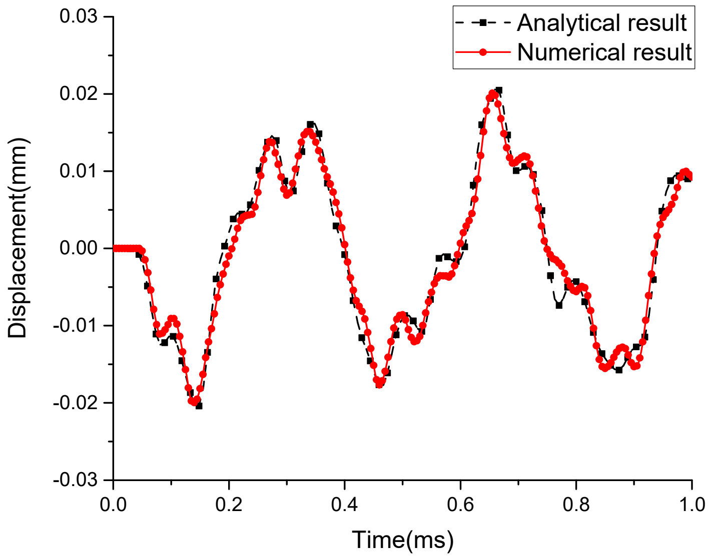

(a)

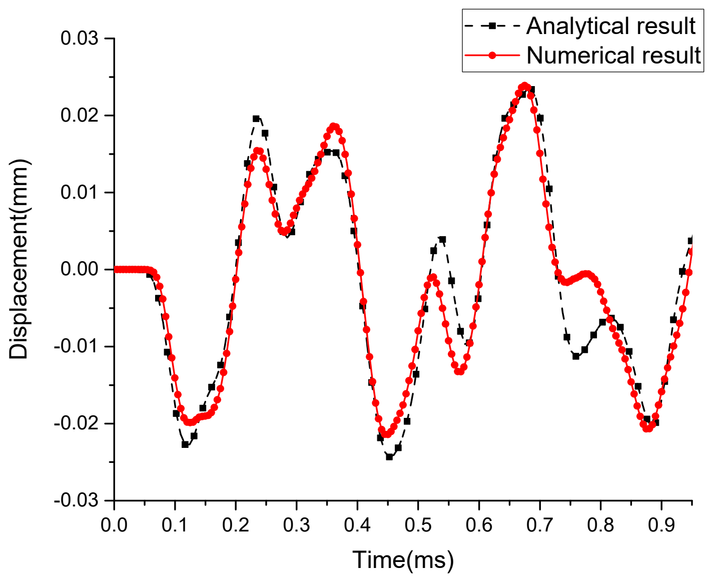

(b)

Fig. 10 Comparison of displacement time history of element 1 and element 2

(a) Element 1, (b) Element 2

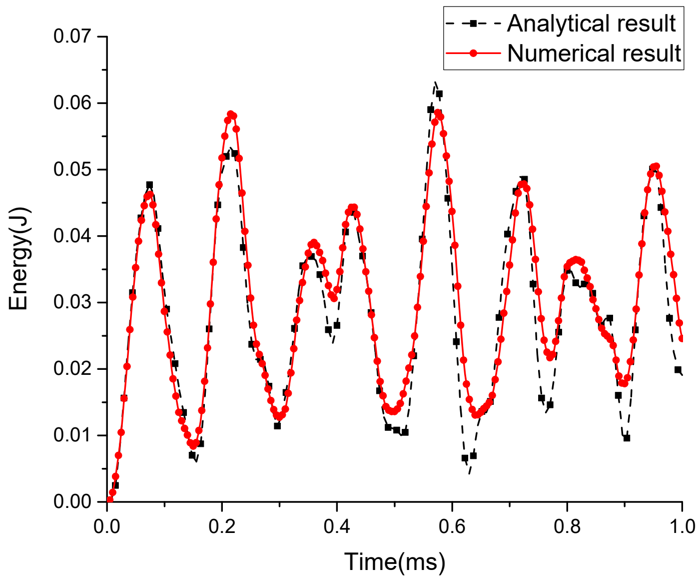

Fig. 11 Comparison of energy time history stored by all the coated lead cores

Fig. 12a and Fig. 12b show the average stress over the sections Cs1 - Cs4 of pure mortar structure and ternary LRC structure, respectively. Fig. 13a - Fig. 13g show the stress contours along the pure mortar structure and ternary LRC structure at different time instants. As shown in Fig. 13a of the stress contour of pure mortar structure at t = 3.748×10^{-2} ms, the compressive stress wave generated by blast loading has not reached the fixed end yet, and the compressive stress wave propagation in the pure mortar structure remains almost unchanged but with a time lag only at different sections, as shown in Fig. 12a of the stress wave at sections Cs1 to Cs3. Fig. 12b shows the wave forms at the same sections in ternary LRC structure. The corresponding stress contour at t = 3.748×10^{-2} ms is shown in Fig. 13b. As shown, the presence of the coated lead cores in ternary LRC structure effectively attenuates the stress in the structure as compared with those shown in Fig. 12a and Fig. 13a. This is because of the stress wave reflection at the interface between the polyurethane coating and the mortar matrix due to the impedance mismatch, as well as the energy storage of lead cores owing to their vibration. With the increase of the number of lead cores passed by stress wave, the peak value of the stress wave is further reduced as shown in Fig. 12b and Fig. 13b. As shown, when the stress wave passes through two lead cores, its peak at section Cs3 is reduced by 30% as compared to the peak value of stress at section Cs1. As shown in Fig. 12a and Fig. 12b, the amplitudes of stress wave in both the pure mortar and ternary LRC structures at section Cs4 are higher. This is because of the wave reflection as section Cs4 is very close to the fixed end of the considered structural model as shown in Fig. 6b. Fig. 13c shows the stress contour of pure mortar structure model. As shown when the compressive stress wave is reflected at the fixed end (t = 7.5×10^{-2} ms), the reflected stress wave is still compressive stress wave because of the fixed end condition. When the incident compressive stress wave and the reflected compressive stress wave superimpose at the fixed end, the peak value of the stress wave in pure mortar structure becomes twice the peak value of the incident stress wave as shown in Fig. 12a. Similarly, Fig. 13d shows the stress contour of ternary LRC structure model when the stress wave is reflected from the fixed end the first time. Due to the energy storage effect of the coated lead cores, the incident compressive wave is smaller as compared to that in the pure mortar structure, as a result the peak value of the compressive stress generated by the superposition of incident and reflected stress wave is reduced by 45% by comparing the first peak value at section Cs4 in Fig. 12a and Fig. 12b. The presence of coated lead cores also obstructs the propagation of stress waves in the mortar matrix, leading to a delayed arrival of the stress wave to section Cs4. A detailed examination of the results shown in Fig. 12 indicates that in the ternary LRC structure, the first arrival time of stress wave to section Cs4 is 2.5×10^{-3} ms delayed than that in the pure mortar structure. Fig. 13e and Fig. 13f show the stress contours of pure mortar and ternary LRC structure when the reflected compressive stress wave from the fixed end reaches the loading application surface. After being reflected from the free surface, the stress wave becomes a tensile wave, and the peak value of the tensile stress is reduced by 71% by comparing the first tensile peak at section Cs1 in Fig. 12a and Fig. 12b, indicating a significant reduction in stress wave amplitude of the ternary LRC structure. As shown in Fig. 12b, the stress wave in ternary LRC structure is less harmonic than that in mortar structure as shown in Fig. 12a. For example, a prominent compressive stress peak appears at section Cs4 in the ternary LRC structure model at t = 0.147 ms, which, however, does not exist in the pure mortar structure. These additional stress wave peaks or small oscillations in ternary LRC structure are caused by the vibrations of lead cores. The secondary compressive wave generated by the lead core vibration superimposes with the reflected compressive wave by the fixed end, resulting in a prominent second compressive stress peak at Cs4.

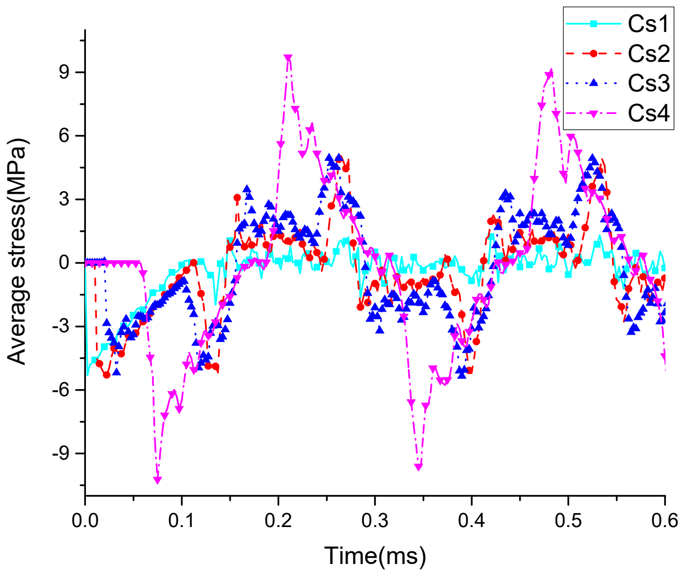

(a)

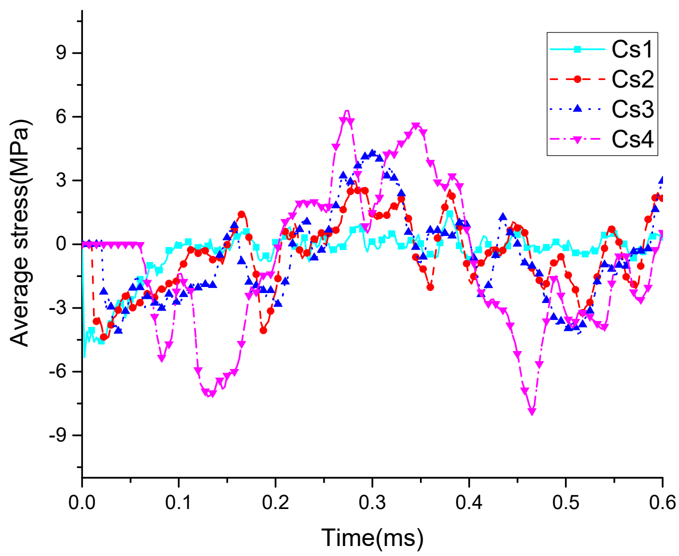

(b)

Fig. 12 Average stress at four cross-sections (a) Pure mortar structure model, (b) Ternary LRC structure model

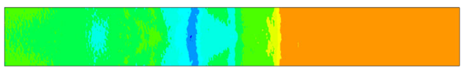
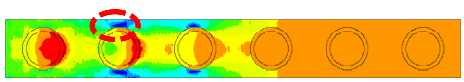

(a) (b)

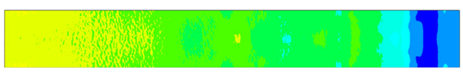
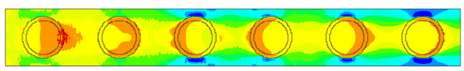

(c) (d)

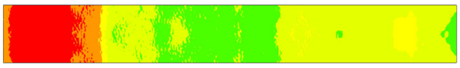

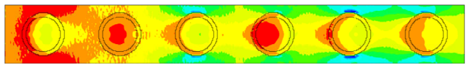

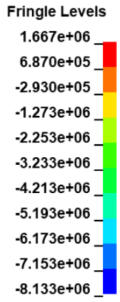

(e) (f)

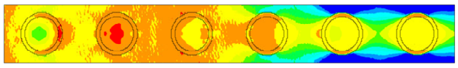

(g)

Fig. 13 Stress contour

(a) Pure mortar, $t = 3.748\times10^{-2}$ ms, (b) Ternary LRC, t = 3.748×10^{-2} ms,

(c) Pure mortar, $t = 7.5\times10^{-2}$ ms, (d) Ternary LRC, $t = 7.75\times10^{-2}$ ms,

(e) Pure mortar, $t = 0.15$ ms, (f) Ternary LRC, $t = 0.16$ ms,

(g) Ternary LRC, $t = 0.147$ ms

The above results demonstrate that the lead cores in mortar matrix can mitigate stress wave propagation in ternary LRC structure. However, it should be noted that the above results are average stress over cross section of the structure. Lead cores in mortar matrix may cause stress concentration at the interfaces between mortar and soft polyurethane coating. To demonstrate this, the stress of element 3 as shown in Fig. 14, which is a mortar element at the interface with the polyurethane coating, is extracted and shown in Fig. 15. As shown, due to the change of material properties in the ternary LRC structure, the local stress concentration in the mortar matrix leads to the local stress value to be three times of the average stress at Cs1. This increase in stress amplitude in ternary LRC structure, which has not been discussed in open literature yet, needs be carefully evaluated when designing the ternary LRC structure as it may lead to localized damage to mortar matrix although the overall stress wave amplitude is reduced.

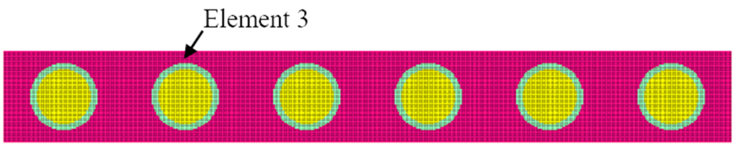

Fig. 14 Location of element 3

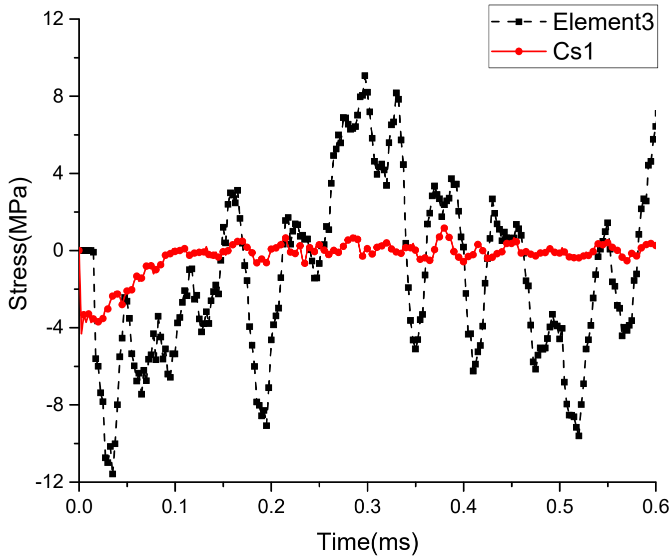

Fig. 15 Stress time history of element 3 and average stress of Cs1

3.6. Parametric investigations

In this section, parametric study is carried out to investigate the influences of various parameters on the effectiveness of ternary LRC structure in mitigating wave propagations. The considered parameters include the material of heavy core, the stiffness and thickness of soft coating.

To study the influence of core material on the response of the ternary LRC structure under blast loading, the responses of ternary LRC structure composed of natural aggregate cores and lead cores are compared. The size of natural aggregate core is the same as that of the lead core. The 5 MPa peak value blast loading is used in the simulation, i.e., the material nonlinearity is not considered. The material parameters of natural aggregate used in the simulation are given in Table 4. In the simulations, all the parameters are kept the same as those in the above, the only variation is the heavy core inclusion.

Table 5 Material parameters of natural aggregate

Material	Density (kg/m^3)	Elastic modulus (MPa)	Poisson's ratio
Natural aggregate	2750	6×10^4	0.25

Fig. 16 compares the velocity of element 2 as shown in Fig. 9 at section Cs5 when core material is natural aggregate and lead, respectively. As shown in Fig. 16, since the polyurethane coating limits the movement of the core, the peak velocity of the natural aggregate core is only slightly higher than that of the lead core under the same loading. Because the density of natural aggregate is smaller than that of lead, the natural aggregate core therefore also vibrates faster with a higher frequency than the lead core.

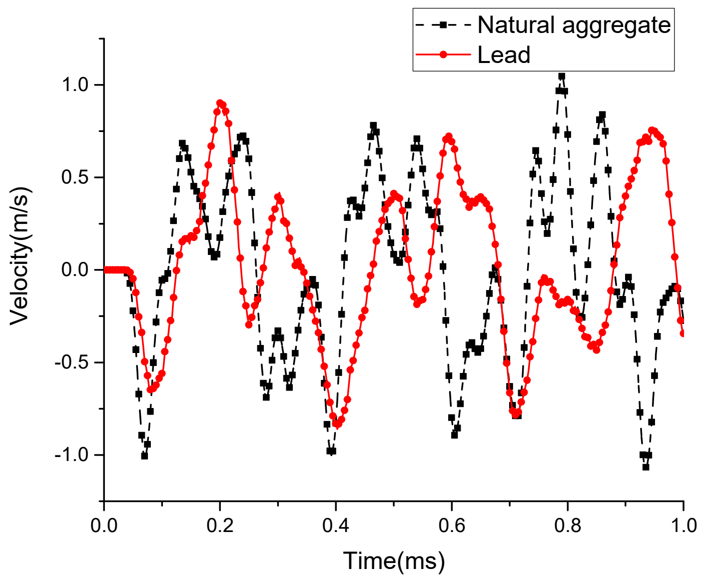

Fig. 16 Velocity time history of element 2

Fig. 17 shows the energy distributions of natural aggregate cores and mortar matrix in ternary LRC structure model. The energy in this figure is the sum of kinetic energy and internal energy for each component. Since the mass of the lead core is larger than that of the natural aggregate and the two cores have similar velocity under the 5 MPa blast loading, the lead cores can store more energy than natural aggregates by comparing with that shown in Fig. 5, which can therefore reduce more energy in the mortar matrix and better mitigate wave propagation in the structure.

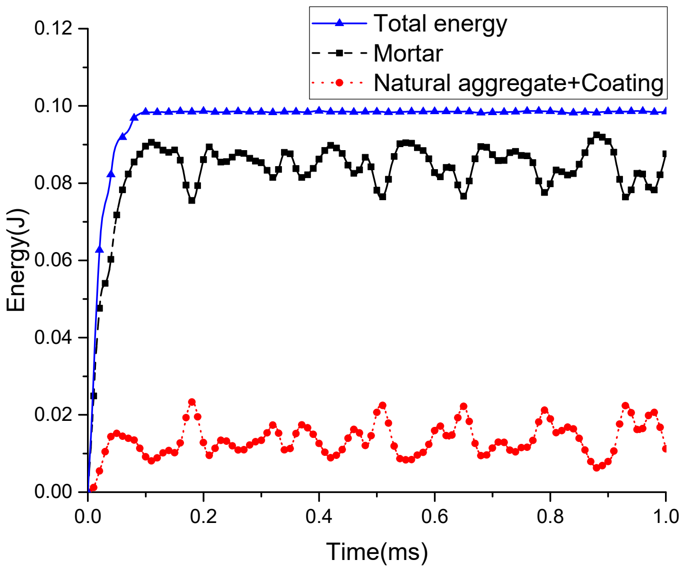

Fig. 17 Energy distribution of ternary LRC structure with natural aggregate core

Fig. 18 shows the average stress in the four designated sections in ternary LRC structure model with natural aggregate cores. Compared with Fig. 12b, it is obvious that lead core is more effective in mitigating stress wave propagation since lead core can store more energy through its vibrations. When the stress wave passes through two natural aggregate cores, the peak stress of section Cs3 is reduced by 11.8% as compared to that of section Cs1, where this value is 30% when lead core is used. Fig. 19a and Fig. 19b show the mortar stress contours of ternary LRC structure model with natural aggregate cores and lead cores at $t = 6.24\times10^{-2}$ ms, respectively. As shown, the change of core material results in a change in the stress distribution of the mortar matrix. The lead core can better reduce the stress in the mortar matrix as compared to natural aggregate core, especially in the middle of the cores (as circled by red dotted line). Therefore, for ternary LRC structure, heavier core is better because it is more effective in reducing the wave propagations.

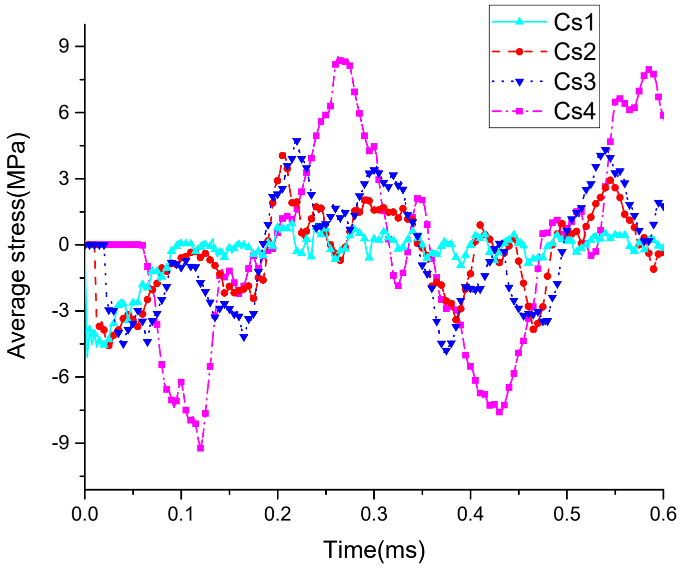

Fig. 18 Average stress in four different cross-sections

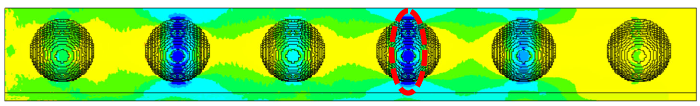

(a)

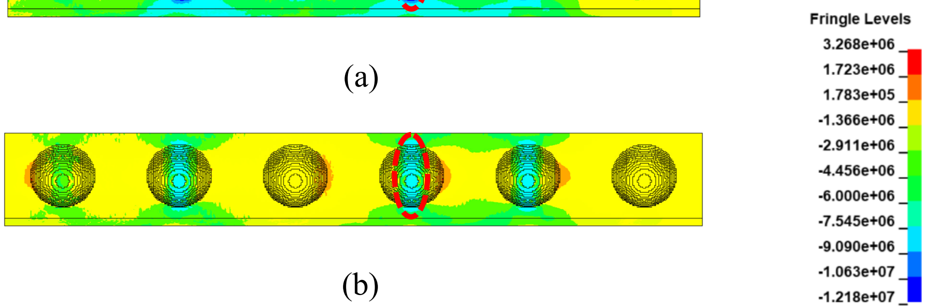

(b)

Fig. 19 Cross-section stress contour of the ternary LRC structure with different core materials at $t = 6.24\times10^{-2}$ ms (a) Natural aggregate core, (b) Lead core

To study the influences of the soft coating stiffness on the performance of ternary LRC structure in mitigating wave propagation, soft coating with three different modulus values, i.e., E_c = 14.7 MPa, E_c = 1.47×10^2 MPa and E_c = 1.47×10^3 MPa, representing very soft, medium and hard coating materials are considered. In the simulations, only the coating modulus is changed while all the other parameters of ternary LRC structure are the same as defined above. Fig. 20a and Fig. 20b show the displacement time histories of element 1 and element 2 when the elastic modulus of polyurethane coating is different. The role of the polyurethane coating in the ternary LRC is to provide space for the lead core to vibrate. By comparing those in Fig. 4, Fig. 20a and Fig. 20b, it is found that the lower the elastic modulus of the polyurethane coating is, the larger the relative displacement between the lead core and the mortar matrix would be. Fig. 21 shows the energy time history of mortar matrix in ternary LRC structure with different elastic modulus of polyurethane coating. The energy in this figure is the sum of kinetic energy and internal energy stored by mortar matrix. As shown, although the relative displacement between heavy core and mortar is the largest when E_c is 14.7 MPa, the mortar matrix has the smallest energy when E_c is 1.47×10^2 MPa, implying the energy stored in heavy core is the largest. This is because when the coating is very soft, i.e., E_c is 14.7 MPa, the energy transferred to the heavy core is small although heavy core relative displacement to the mortar matrix is large but it vibrates slower with lower frequency and velocity as compared to the case when E_c is 1.47×10^2 MPa. On the other hand, when the heavy core is very stiff, i.e., E_c is 1.47×10^3 MPa in the considered examples in the present study, the heavy core can hardly vibrate by itself and the relative displacement between the core and mortar matrix is very small, hence the stored energy by the heavy core is also small.

Therefore, to achieve the best performance of ternary LRC structure in mitigating wave propagation, proper analysis is needed to determine the best coating materials with suitable modulus.

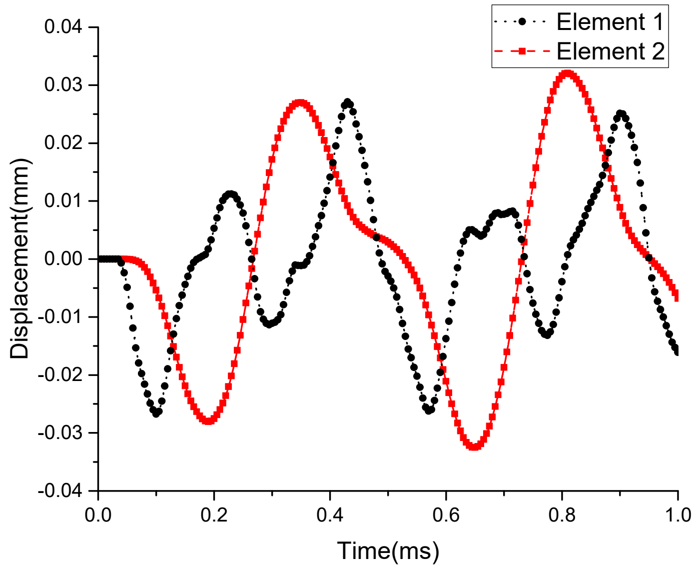

(a)

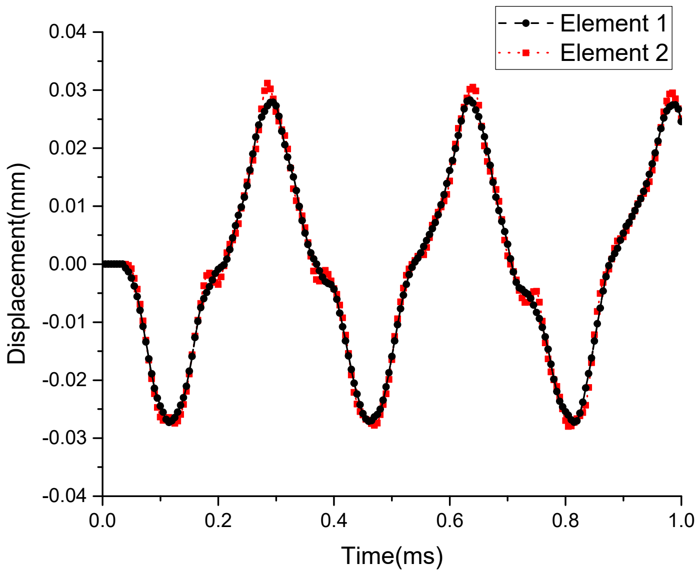

(b)

Fig. 20 Displacement time histories of the two elements at section Cs5

(a) $E_c = 14.7$ MPa, (b) $E_c = 1.47\times10^3$ MPa

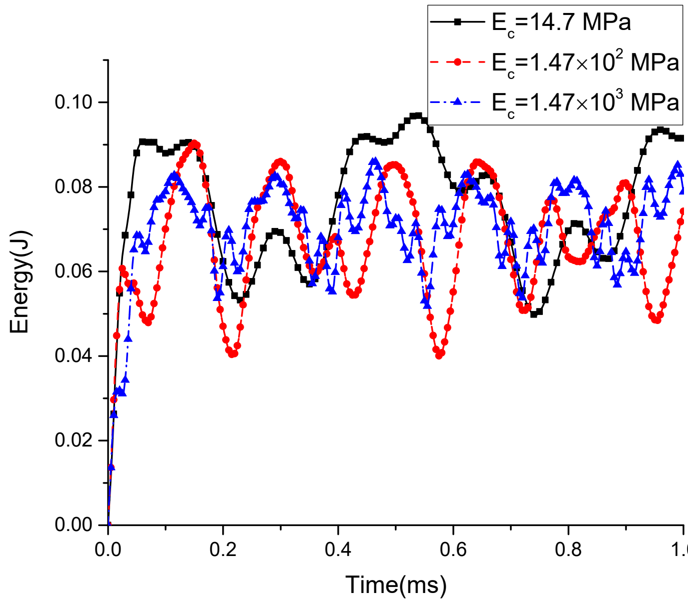

Fig. 21 Energy stored by mortar matrix corresponding to different coating E_c

Fig. 22 shows the stress contours of mortar matrix with the coatings of different elastic modulus at t = 6.5×10^{-2} ms. As shown, the lower the elastic modulus of the coating is, the more obvious the stress concentration in the mortar matrix around the coated lead cores with larger compressive stress would be, as indicated by red dotted line. When E_c is 1.47×10^3 MPa, the coated lead core has better resistance to deformation and the stress concentration is less prominent, its energy storage ability is lower, therefore is less effective in mitigating stress wave propagation. These results indicate again that proper analysis is needed to determine the coating stiffness to achieve the best balance between wave mitigation and less stress concentration to minimize the localized damage in ternary LRC structure.

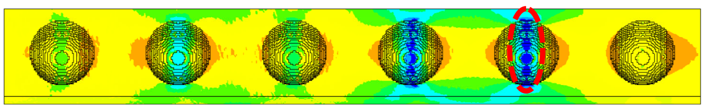

(a)

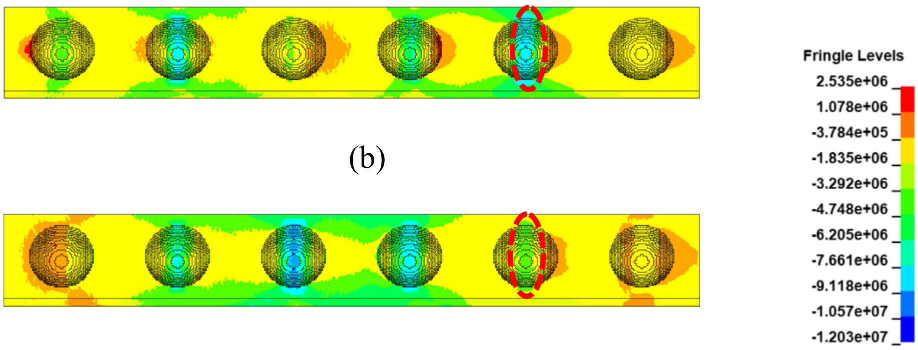

(b)

(c)

Fig. 22 Stress contour of mortar matrix with different E_c at $t = 6.5\times10^{-2}$ ms

(a) $E_c = 14.7$ MPa, (b) $E_c = 1.47\times10^2$ MPa, (c) $E_c = 1.47\times10^3$ MPa

To investigate the influence of coating thickness on the effectiveness of ternary LRC structure in mitigating wave propagation, three coating thicknesses, namely b = 0 mm, i.e., no coating, b = 2 mm and b = 4 mm, are considered. In the simulations, all the ternary LRC structure parameters, except the coating thickness, are kept the same as defined above. Fig. 23 shows the energy time history of mortar matrix in ternary LRC structure model under different polyurethane coating thicknesses. The energy in this figure is the sum of kinetic energy and internal energy stored by mortar matrix. Fig. 24 shows the stress contour of ternary LRC structure at $t = 5.72\times10^{-2}$ ms. When the lead core in the mortar matrix is not coated, the lead core can store parts of the energy applied by the blast loading. As shown, the energy in the mortar matrix varies between 0.0615 J and 0.0902 J. Polyurethane coating outside the lead core effectively increases the ability of the core to store energy, thereby reducing the energy and the stress in the mortar matrix. When b = 2 mm and b = 4 mm, the minimum energy in the mortar matrix is reduced by 34.8% and 22% as compared to that when b = 0 mm, respectively. As can be noted, among the three considered cases, when b = 2 mm, the ternary LRC structure performs the best in reducing wave propagation. When b = 4 mm, the performance of the structure is not as good as compared to the case when b = 2 mm. This is again because the coating layer becomes too soft when b = 4 mm, which reduces the wave energy being transferred to the heavy core owing to the filtering effect and also makes the heavy core vibrate at smaller velocity, thus the energy stored by the heavy core is less compared to the case when b = 2 mm. The addition of the polyurethane coating also causes significant stress concentration (Red dotted line) at the interface between the mortar matrix and the polyurethane coating, as shown in Fig. 24, which may lead to localized damage to the ternary LRC structure. These results, together with those presented above, indicate that coating layer thickness and stiffness need be properly determined to achieve the best performing ternary LRC structure in mitigating wave propagation and stress concentration at the interface between mortar matrix and heavy core inclusion.

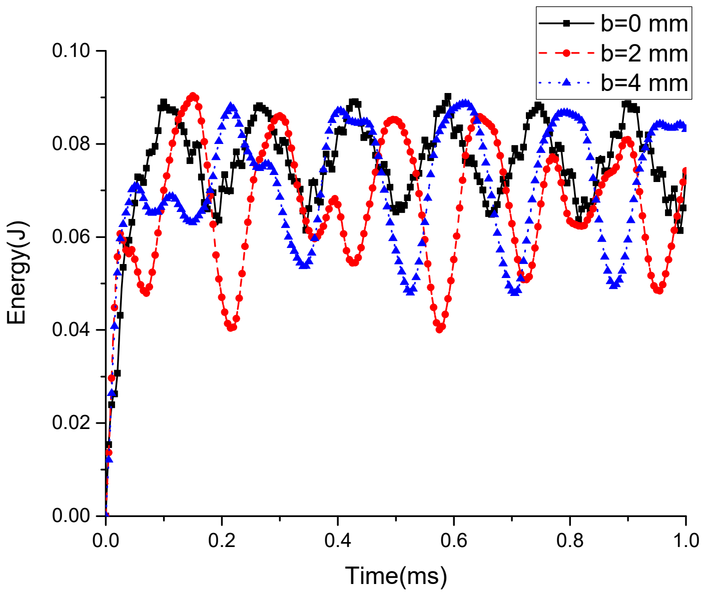

Fig. 23 Energy stored by mortar in LRC with different soft coating thickness

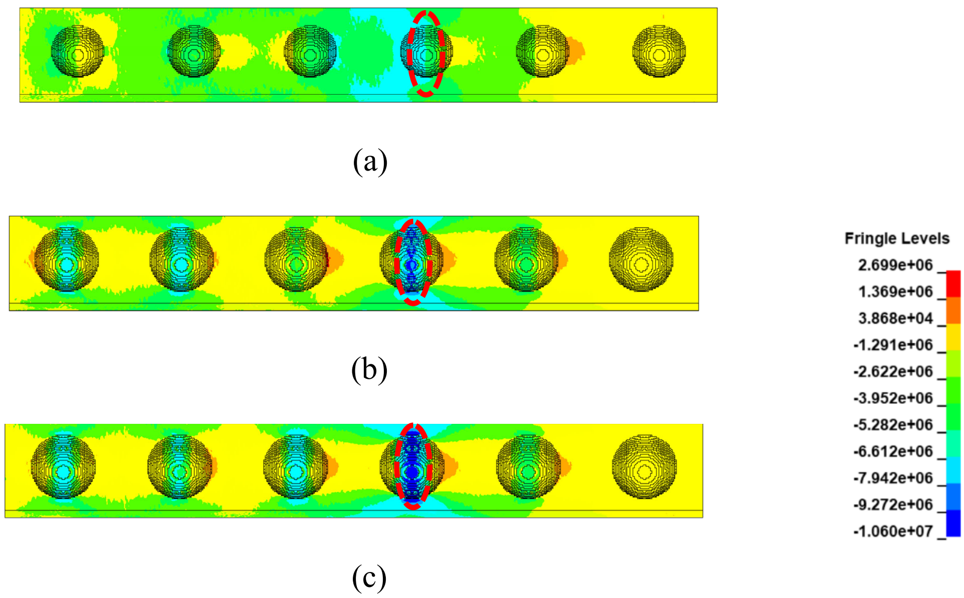

Fig. 24 Stress contour of mortar matrix with respect to different coating thickness at $t = 5.72\times10^{-2}$ ms (a) $b = 0$ mm, (b) $b = 2$ mm, (c) $b = 4$ mm

3.7. Coupled effect of material damage and mechanism of ternary LRC

To investigate the coupled effect of material damage and local resonating mechanism of ternary LRC on mitigating blast waves in concrete, the blast loading of 20 MPa and 40MPa amplitude are considered. The material parameters and the geometric parameters of the ternary LRC structure model are the same as given in Table 1-Table 3.

Fig. 25a and Fig. 25b show the average stress over the sections Cs1 - Cs4 of pure mortar structure and ternary LRC structure under the blast loading of 20 MPa amplitude, respectively. As shown, the largest compressive and tensile stress occurs at the fixed end, i.e., near Cs4, owing to the wave reflection. Due to the energy storage of the coated lead cores, the first peak compressive stress at the section Cs4 in the ternary LRC structure is reduced by 53.9% as compared to that of the pure mortar structure. Because of the reduction in stress wave amplitude, complete failure of ternary LRC structure at the fixed end does not occur. The stress wave therefore continues to propagate back and forth in the structure until gradually damps out as shown in Fig. 25b. The section Cs4 in pure mortar structure is not damaged by the first reflected compressive stress from the fixed end, however, is damaged by the reflected tensile stress, which leads to the quick drop of the stress in the section to zero as shown in Fig. 25a. The tensile stress is generated by the reflection at the free end and propagates in the structure, which is intensified by the reflection from the fixed end and caused the damage at the section Cs4. Fig. 26a shows the stress contour of pure mortar structure before it is damaged at t = 0.2 ms. As shown, the fixed end subjects to tensile stress reflected from the free end. The tensile stress wave increases owing to the reflection from the fixed end, leads to the failure at the fixed end of the pure mortar structure at t = 0.21 ms as shown in Fig. 26b. It should be noted that although the tensile stress amplitude in other sections exceeds the static tensile strength of the mortar material, failure only occurs at the fixed end because the strain rate effect on mortar material strength is considered in the simulation, which enhanced the mortar tensile strength. After the tensile damage at the fixed end, the stress in section Cs4 becomes zero, and the damaged section becomes a free end because of the erosion of the damaged material in simulation. The subsequent tensile stress wave becomes a compressive stress wave owing to the free end reflection as shown in Fig. 26b.

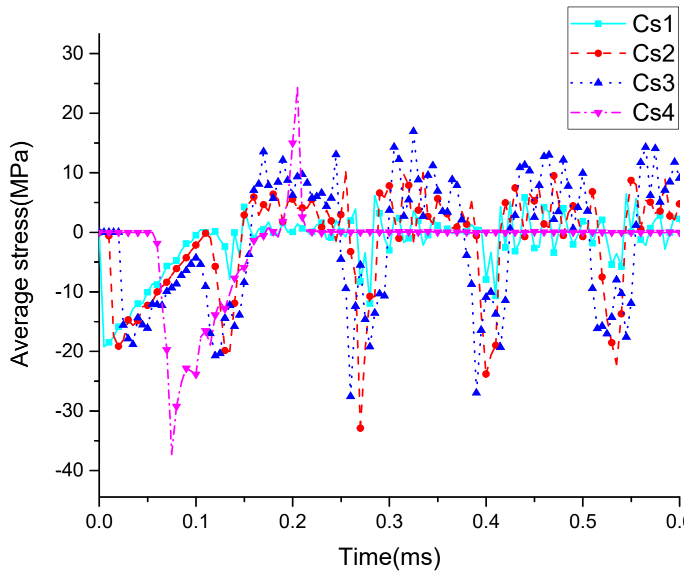

(a)

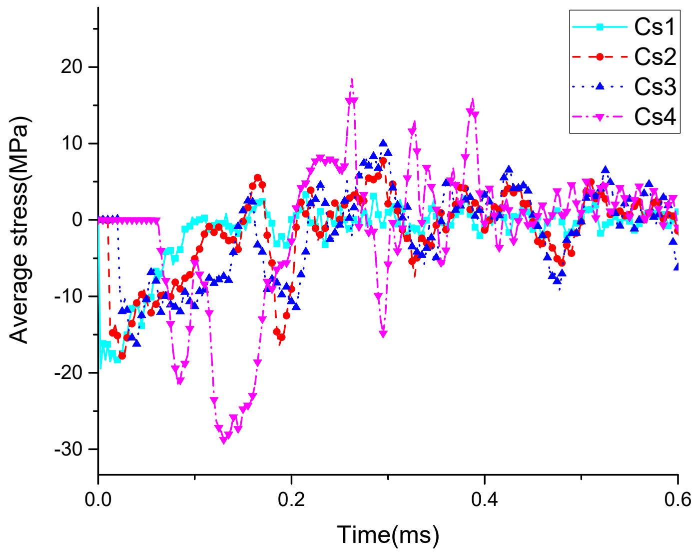

(b)

Fig. 25 Average stress in the four sections under blast loading of 20 MPa amplitude

(a) Pure mortar structure, (b) Ternary LRC structure

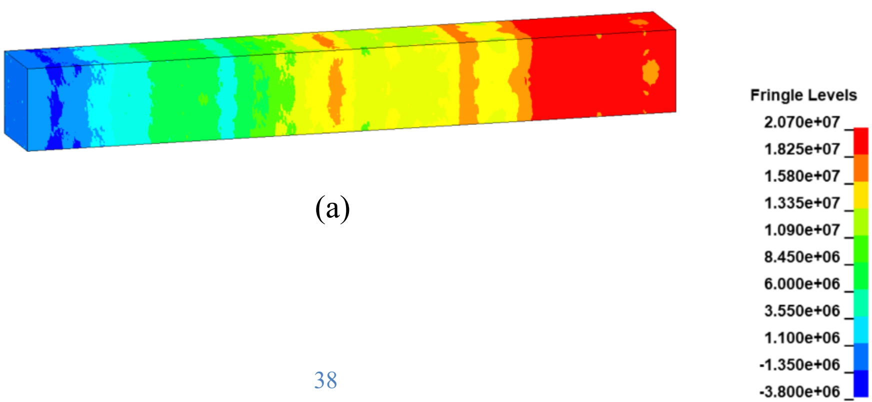

(a)

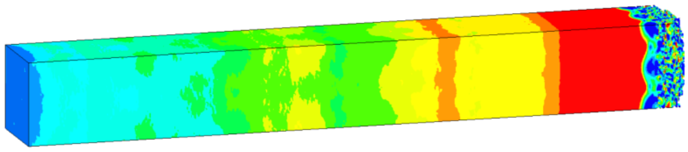

(b)

Fig. 26 Failure pattern of pure mortar structure (a) t = 0.2 ms, (b) t = 0.21 ms

Fig. 27a shows the failure pattern of ternary LRC structure at t = 0.239 ms under the blast loading of 20 MPa amplitude. Fig. 27b shows the stress contour of the mid-section of the structure at t = 0.237 ms before the structure is damaged. As shown, at t = 0.237 ms, the area near the fourth heavy core inclusion in the present considered model experiences large tensile stress. This tensile stress causes damage to the mortar material, but does not damage the core inclusion. The tensile stress continues to propagate in the structure. Fig. 29 shows the displacements of a mortar element 4 and a lead element 5 (location defined in Fig. 28), located at the section of the fourth heavy core where mortar failure happens as indicated in Fig. 27a. As shown, the moving direction of the two elements at t = 0.237 ms is opposite to the initial direction, i.e., positive displacement vs negative displacement, and the displacement of the lead element is larger than that of the mortar element. The mortar matrix experiences significant tensile stress owing to stress concentration at the mortar-inclusion interface, which leads to tensile failure of mortar material. Although the mortar matrix in the ternary LRC structure breaks in the middle of the model, the stress wave is still transmitted by the coated lead core.

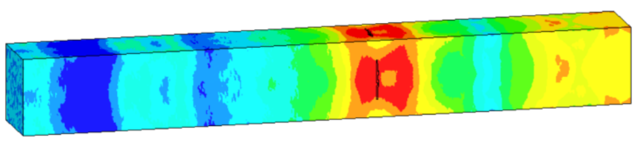

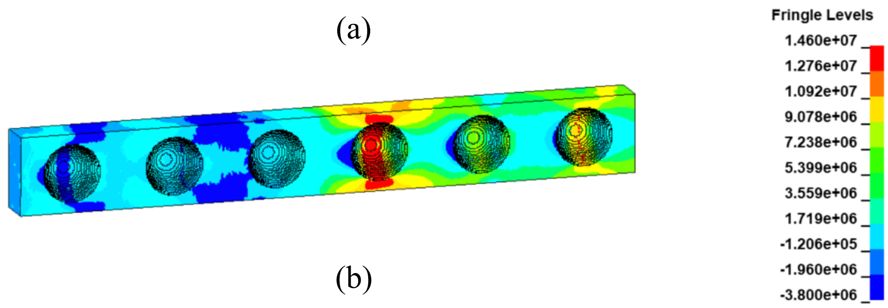

Fig. 27 Failure pattern of ternary LRC structure (a) t = 0.239 ms, (b) t = 0.237 ms

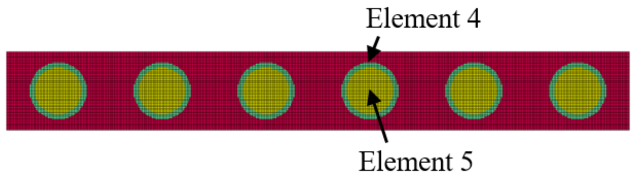

Fig. 28 Location of element 4 and element 5

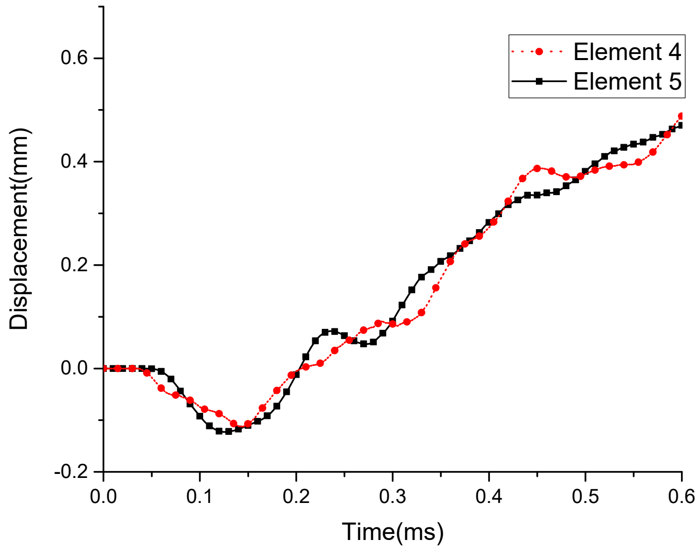

Fig. 29 Displacement time histories of element 4 and element 5

Fig. 30a and Fig. 30b show the average stress of the sections Cs1 - Cs4 of pure mortar structure and ternary LRC structure under the blast loading of 40 MPa amplitude, respectively. As shown in Fig. 30a, the compressive stress of Cs4 in pure mortar structure is doubled when the stress wave reaches the fixed end at the first time. Because the strain rate effect on mortar material strength is considered in the simulation, no compressive failure occurs at the fixed end although the compressive stress is substantially larger than the static strength of considered mortar material. The reflected compressive stress wave continues to propagate back and becomes tensile stress wave when reflected by the free surface on the loading end. Due to the low tensile strength of mortar, the pure mortar structure is broken at t = 0.182 ms as shown in Fig. 30a at a section close to Cs3. As can be noticed in Fig. 30a, the reflected tensile stress from the free surface in mortar structure increases with wave propagation instead of attenuates. This interesting phenomenon has been observed in many previous concrete spalling tests with Split Hopkinson Pressure Bar [33, 37]. In spalling tests, due to the wave superposition of the original compressive wave and the reflected tensile wave, the net tensile wave leads to spalling of the specimen at a certain distance from the free surface, where the net tensile stress exceeds the critical failure stress of the specimen. The location of tensile failure section depends on the tensile stress amplitude, dynamic tensile strength of the specimen, and the wave length of stress wave. The first tensile failure of the mortar structure model in this study locates at a section of 0.095 m from the free surface as shown in Fig. 31a. After the broken up of the specimen, stress wave continues propagating in both parts of the broken segments. Tensile failure also occurs at the fixed end near Cs4, which is not shown here. As shown in Fig. 30a, after the structure broken into two pieces, the stress wave at sections Cs1-Cs3 oscillates faster and becomes more harmonic. This is because the broken segment is shorter than the original structure model, and both ends of the broken segments are now free and therefore stress wave changes direction due to the free surface reflection. Fig. 31b and Fig. 31c show the failure pattern of the ternary LRC structure at $t = 2.24\times10^{-2}$ ms. As shown, compressive damage occurs at the interface between the mortar matrix and the polyurethane coating owing to stress concentration. The damage at the loading end substantially reduces stress wave energy, which causes the stress of the subsequent sections to be greatly attenuated. For example, the first compressive stress peaks of Cs3 and Cs4 are reduced by 44.3% and 78.3%, respectively, as compared to the 30% and 45% reduction at the same sections shown in Fig. 12b when no material damage is considered and the wave attenuation is caused only by ternary mechanism. These results indicate that localized damage near the heavy cores could absorb significant amount of wave energy and localize the structural damage, which could be a merit for using metamaterial to make protective structures. Together with the wave mitigation mechanism of the ternary LRC structure, the localized damage could be beneficial for structure protection if the structure is properly designed and damage is properly controlled.

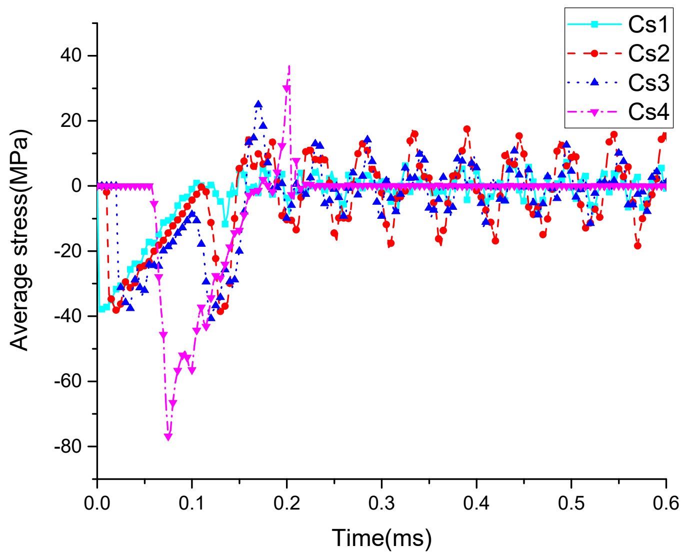

(a)

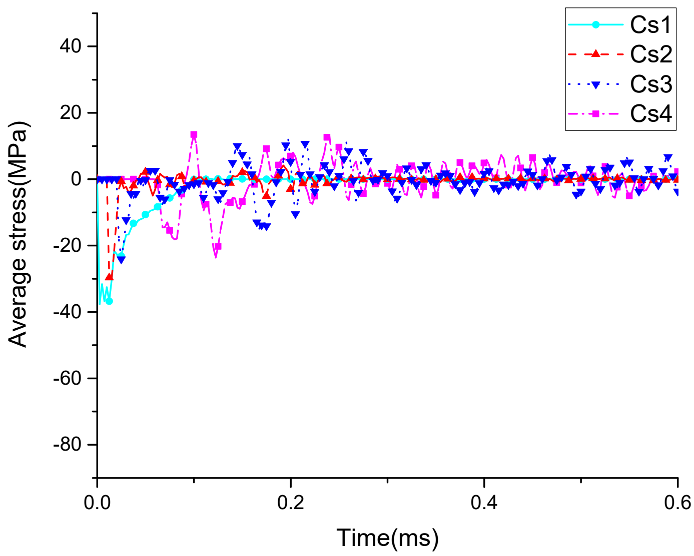

(b)

Fig. 30 Average stress in four cross sections under blast loading of 40 MPa amplitude (a) Pure mortar structure, (b) Ternary LRC structure

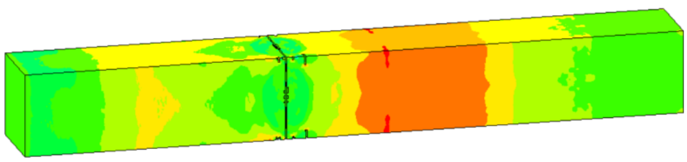

(a)

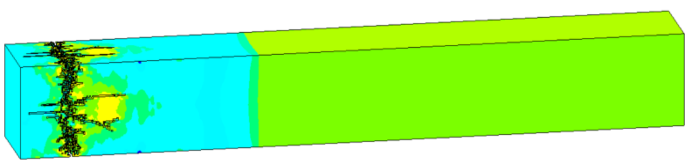

(b)

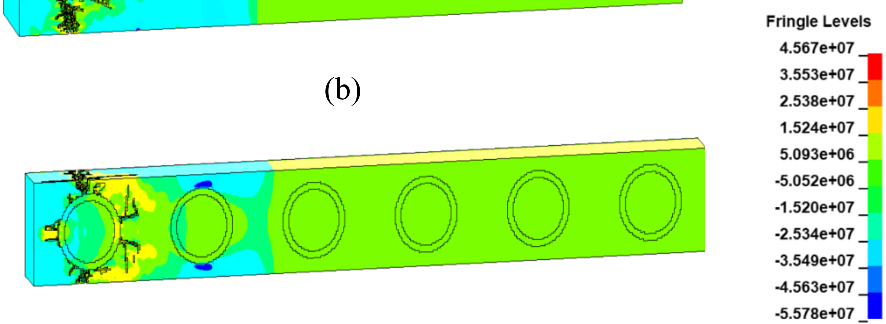

(c)

Fig. 31 Failure pattern and stress contour of pure mortar structure and ternary LRC structure (a) Pure mortar structure, t = 0.182 ms, (b) Ternary LRC structure, t =

2.24×10^{-2} ms, (c) Cross-section of ternary LRC structure

4. Conclusions

In the present study, the performance of ternary LRC structure comprising spherical lead inclusion and soft coating in mortar matrix subjected to blast loads is studied. Both analytical derivation and numerical modelling are carried out to study the mechanism and performance of ternary LRC in mitigating blast loading induced stress wave propagation in the structure. The results show that ternary LRC structure can mitigate stress wave propagation because of the relative movement between heavy inclusion and mortar matrix, and vibration of heavy inclusions. The heavier is the inclusion, the more effective is the structure in reducing the stress wave propagation because the vibration of heavy inclusion stores more wave energy. The soft coating provides space for the vibration of the heavy inclusion, but very soft coating layer prevents wave energy being transmitted to the heavy core inclusion, therefore could be less effective in mitigation of stress wave propagation. Existence of soft coating and heavy core in mortar matrix also causes stress concentration at the interface, which may lead to localized damage. The material damage, together with the local resonating mechanism of ternary LRC, however, makes the structure more effective in mitigating blast-induced stress waves because the localized damage can absorb a significant amount of energy. Therefore proper analysis is needed to find the best possible designs of heavy inclusion and soft coating in mortar matrix to achieve the most effective ternary LRC structure for structural protection.

5. Acknowledgement

The authors are grateful for the financial support from the Australian Research Council (ARC) for Laureate Fellowships FL180100196.

References:

[1] V.G. Veselago, The electrodynamics of substances with simultaneously negative values of ε and μ, Soviet Physics Uspekhi 10(4) (1968) 509-514.

[2] J.B. Pendry, Negative refraction makes a perfect lens, Physical review letters 85(18) (2000) 3966.

[3] T. Tanaka, A. Ishikawa, S. Kawata, Unattenuated light transmission through the interface between two materials with different indices of refraction using magnetic metamaterials, Physical Review B 73(12) (2006) 125423.

[4] M.S. Kushwaha, P. Halevi, L. Dobrzynski, B. Djafari-Rouhani, Acoustic band structure of periodic elastic composites, Physical review letters 71(13) (1993) 2022.

[5] A. Klironomos, E. Economou, Elastic wave band gaps and single scattering, Solid state communications 105(5) (1998) 327-332.

[6] G. Wang, J. Wen, Y. Liu, X. Wen, Lumped-mass method for the study of band structure in two-dimensional phononic crystals, Physical Review B 69(18) (2004) 184302.

[7] M. Hirsekorn, Small-size sonic crystals with strong attenuation bands in the audible frequency range, Applied Physics Letters 84(17) (2004) 3364-3366.

[8] Z. Cheng, Z. Shi, Novel composite periodic structures with attenuation zones, Engineering Structures 56 (2013) 1271-1282.

[9] Z. Liu, X. Zhang, Y. Mao, Y. Zhu, Z. Yang, C. Chan, P. Sheng, Locally resonant sonic materials, science 289(5485) (2000) 1734-1736.

[10] Z. Liu, C. Chan, P. Sheng, Three-component elastic wave band-gap material, Physical Review B 65(16) (2002) 165116.

[11] J. Hsu, T. Wu, Lamb waves in binary locally resonant phononic plates with two-dimensional lattices, Applied physics letters 90(20) (2007) 201904.

[12] Z. Li, H. Chen, The development trend of advanced building materials, Proceeding of the first international forum on advances in structural engineering, 2006.

[13] Z. Cheng, Z. Shi, Y. Mo, H. Xiang, Locally resonant periodic structures with low-frequency band gaps, Journal of Applied Physics 114(3) (2013) 033532.

[14] Y. Yan, A. Laskar, Z. Cheng, F. Menq, Y. Tang, Y. Mo, Z. Shi, Seismic isolation of two dimensional periodic foundations, Journal of Applied Physics 116(4) (2014) 044908.

[15] S.A. Asiri, Y.Z. AL-Zahrani, Theoretical Analysis of Mechanical Vibration for Offshore Platform Structures, World Journal of Mechanics 4(1) (2014) 1.

[16] H. Hao, Y. Hao, J. Li, W. Chen, Review of the current practices in blast-resistant analysis and design of concrete structures, Advances in Structural Engineering 19(8) (2016) 1193-1223.

[17] H. Jin, W. Chen, H. Hao, Y. Hao, Numerical study on impact resistance of metaconcrete (in Chinese), Science China (Physics, Mechanics & Astronomy) 49 (2019).

[18] Y. Hao, H. Hao, Y. Shi, Z. Wang, R. Zong, Field testing of fence type blast wall for blast load mitigation, International Journal of Structural Stability Dynamics 17(09) (2017) 1750099.

[19] X. Zhou, H. Hao, Prediction of airblast loads on structures behind a protective barrier, International Journal of Impact Engineering 35(5) (2008) 363-375.

[20] N. Gebbeken, Urbane Sicherheit bei Explosionen–Schutz durch Bepflanzung, Bautechnik 94(5) (2017) 295-306.

[21] C. Yuan, W. Chen, T.M. Pham, H. Hao, Effect of aggregate size on bond behaviour between basalt fibre reinforced polymer sheets and concrete, Composites Part B: Engineering 158 (2019) 459-474.

[22] Y. Huang, Y. Guo, Review of durability of Fiber Reinforced Polymer (FRP) reinforced concrete structure, Applied Mechanics and Materials, Trans Tech Publ, 2014, pp. 1651-1654.

[23] M.H. Klaus, Response of a panel wall subjected to blast loading, Computers Structures 21(1-2) (1985) 129-135.

[24] S.J. Mitchell, A. Pandolfi, M. Ortiz, Metaconcrete: designed aggregates to enhance dynamic performance, Journal of the Mechanics Physics of Solids 65 (2014) 69-81.

[25] S.J. Mitchell, A. Pandolfi, M. Ortiz, Investigation of elastic wave transmission in a metaconcrete slab, Mechanics of Materials 91 (2015) 295-303.

[26] S.J. Mitchell, A. Pandolfi, M. Ortiz, Effect of brittle fracture in a metaconcrete slab under shock loading, Journal of Engineering Mechanics 142(4) (2016) 04016010.

[27] K.T. Tan, H. Huang, C. Sun, Blast-wave impact mitigation using negative effective mass density concept of elastic metamaterials, International Journal of Impact Engineering 64 (2014) 20-29.

[28] Z. Liu, C. Chan, P. Sheng, Analytic model of phononic crystals with local resonances, Physical Review B 71(1) (2005) 014103.

[29] H. Huang, C. Sun, G. Huang, On the negative effective mass density in acoustic metamaterials, International Journal of Engineering Science 47(4) (2009) 610-617.

[30] C. Kettenbeil, G. Ravichandran, Experimental investigation of the dynamic behavior of metaconcrete, International Journal of Impact Engineering 111 (2018) 199-207.

[31] G.W. Milton, J.R. Willis, On modifications of Newton's second law and linear continuum elastodynamics, Proceedings of the Royal Society A: Mathematical, Physical Engineering Sciences 463(2079) (2007) 855-880.

[32] C. Yi, P. Zhang, D. Johansson, U. Nyberg, Dynamic response of a circular lined tunnel with an imperfect interface subjected to cylindrical P-waves, Computers Geotechnics 55 (2014) 165-171.

[33] G. Chen, Y. Hao, H. Hao, 3D meso-scale modelling of concrete material in spall tests, Materials Structures 48(6) (2015) 1887-1899.

[34] Y. Hao, H. Hao, Z. Li, Numerical analysis of lateral inertial confinement effects on impact test of concrete compressive material properties, International Journal of Protective Structures 1(1) (2010) 145-167.

[35] Y. Hao, H. Hao, G. Jiang, Y. Zhou, Experimental confirmation of some factors

influencing dynamic concrete compressive strengths in high-speed impact tests, Cement concrete research 52 (2013) 63-70.

[36] L. Malvar, J. Crawford, Dynamic increase factors for concrete. In: Twenty-eighth DDESB seminar, Orlando, Florida (1998).

[37] H. Wu, Q. Zhang, F. Huang, Q. Jin, Experimental and numerical investigation on the dynamic tensile strength of concrete, International Journal of Impact Engineering 32(1-4) (2005) 605-617.